American Mineralogist, Volume 67, pages 917–925, 1982

Petrology of kimberlite from the DeBruyn and Martin Mine, Bellsbank, South Africa

NABIL Z. BOCTOR and F. R. BOYD

Geophysical Laboratory
Carnegie Institution of Washington
Washington, D. C. 20008

Abstract

The micaceous kimberlite from DeBruyn and Martin Mine, Bellsbank, South Africa, is composed of olivine, phlogopite, spinels, and perovskite in a groundmass of calcite and phlogopite. Three types of phlogopite are present: macrocrysts [Mg/(Mg+Fe) ≃ 0.93, FeO (3–3.5 wt.%), TiO_2 (0.5–0.7 wt.%), Cr_2O_3 (0.4–0.45 wt.%), low Fe_2O_3, ΔT (Fe^{3+} in tetrahedral sites = 0.01–0.05]; groundmass phlogopite [Mg/(Mg+Fe) ≃ 0.88, FeO (≃ 6.0 wt.%), TiO_2 (≃ 1.5 wt.%), Cr_2O_3 (0.5–0.6 wt.%), high Fe_2O_3, ΔT = 0.429–0.666]; and phlogopite aggregates associated with olivine xenocrysts [Mg/(Mg+Fe) ≃ 0.90, FeO (4.5–5 wt.%), TiO_2 (0.4–0.7 wt.%), no ferric iron, and high Cr_2O_3 (2.7–3.4 wt.%)]. The phlogopite macrocrysts crystallized from the kimberlite magma prior to emplacement; groundmass phlogopite appears to have crystallized from late-stage kimberlitic fluids after emplacement; and the phlogopite aggregates are products of disaggregation of ultramafic nodules. Spinels show crystallization trends different from those of mica-poor "basaltic kimberlites." The Mg–Al chromite is the earliest spinel to crystallize and is followed by titaniferous magnesian chromite and titaniferous magnetite. The crystallization trend is toward decrease in Al_2O_3 and increase in TiO_2 and Fe_2O_3. The sharp decrease in Al_2O_3 content from Mg–Al chromite to titaniferous chromite is attributed to the crystallization of groundmass phlogopite, which depleted the kimberlitic liquid in Al. Perovskite shows a remarkable enrichment in REE and Nb relative to other South African kimberlites. Perovskite also is highly enriched in LREE and appears to be the major REE-bearing phase in kimberlite from the DeBruyn and Martin Mine. The high concentrations of REE and other incompatible elements in this kimberlite and the wide range of concentrations displayed by these elements in different kimberlites from the Bellsbank region suggest that kimberlite magma was derived from a garnet lherzolite source that was affected by metasomatism in the upper mantle via equilibration with LREE-enriched CO_2 and H_2O vapors.

Introduction

A large number of kimberlite dikes occur in the Barkley West district of the Cape Province. One set of these dikes, the Bellsbank dikes, was emplaced in dolomite of the Campbell-Rand series along two main fissure systems that strike NE–SW and are several kilometers long and several kilometers apart. The fissure system in which the DeBruyn and Martin Mine is located is known as the main fissure system. The other one is commonly known as the Bobbejaan fissure. The fissures in the Bellsbank region are less than 1 m thick; their dip is nearly vertical and they appear to have formed by the widening and infilling of joint systems in the host rock by kimberlitic magma.

The kimberlite from DeBruyn and Martin Mine is a micaceous kimberlite that is characterized by high concentrations of REE and other incompatible elements relative to other South African kimberlites (Fesq *et al.*, 1975; Kable *et al.*, 1975). It is also the richest in these elements among the kimberlite dikes at Bellsbank. The present investigation involves a study of the petrology, mineral chemistry, and opaque mineralogy of the micaceous kimberlite from DeBruyn and Martin Mine and a discussion of the possible mechanisms that led to the enrichment of the REE and other incompatible elements in this kimberlite.

Methods of study

The specimens were studied in both reflected and transmitted light. Analyses were performed with an automated MAC-500 electron microprobe. The cor-

0003–004X/82/0910–0917$02.00

recting schemes of Bence and Albee (1968) and Albee and Ray (1970) were used for data reduction of the silicate and oxide phases. The MAGIC IV computer program of Colby (1971) was used for data reduction of perovskite analyses by the technique described by Boctor and Boyd (1980).

Petrography and mineral chemistry

The petrography of kimberlite from the Bellsbank dikes has been described by Bosch (1971), who considered the kimberlite "as a phlogopite-carbonate rock containing 'xenocrystic olivine.' " Bosch reported a high concentration of phlogopite in the groundmass (19–54% by volume), which confirms its micaceous nature.

The kimberlite from the DeBruyn and Martin Mine is composed of olivine, phlogopite, spinels, and perovskite in a carbonate-phlogopite groundmass. Olivine occurs mostly as large xenocrysts (Fig. 1a) (up to 3 mm in size), as well as euhedral crystals (Fig. 1b) in the groundmass. The xenocrysts have a forsterite content of 89.7–92.2 (Table 1) and tend to be more iron-rich toward their serpentinized margins. Euhedral olivine crystals in the groundmass have a forsterite content of 89.7–91.8 and do not seem to differ from the xenocrysts in their major element chemistry. The euhedral nature of the olivine in the groundmass, however, suggests that it crystallized from the kimberlite magma. The olivine contains minor amounts of Ni in solid solution (0.1–0.6 wt.%), and heazlewoodite (Ni_3S_2) occurs as a secondary sulfide in the serpentinized portions.

Phlogopite occurs as macrocrysts, as a groundmass mineral, and as aggregates associated with large olivine xenocrysts. The macrocrysts are ≃ 1–1.5 mm in size; they are highly deformed (Fig. 1b) and show prominent kinking. The macrocrysts show little compositional variation (Table 2) and are characterized by their high MgO content (25–26 wt.%) [Mg/(Mg+Fe) ≃ 0.93], low FeO content (3–3.5 wt.%), and low TiO_2 content (0.5–0.7 wt.%). A few phlogopite macrocrysts show compositional zoning (Fig. 1d) with the rims being slightly enriched in FeO but more enriched in TiO_2 and Al_2O_3 and more depleted in Cr_2O_3 relative to the cores (Table 2). The cores show the reverse pleochroism described by Farmer and Boettcher (1981), whereas the rims show normal pleochroism. These authors suggested that the pleochroism of phlogopite may be controlled by the available Si + Al + Ti; the sum of these cations is less than 8 for the reverse cores and greater than 8 for the normal rims. Groundmass phlogopite is enriched in FeO (≃ 6.0 wt.%) and TiO_2 (≃ 1.5 wt.%) but depleted in Al_2O_3 relative to the unzoned macrocrysts (Table 2).

The phlogopite aggregates differ in composition from both macrocrysts and groundmass phlogopite in being richer in Al_2O_3 (14.2–15.2 wt.%) and Cr_2O_3 (1.7–3.4 wt.%) but show lower MgO content (22–23.3 wt.%).

Calculation of ΔT, a parameter defined by Smith *et al.* (1978) to equal 8 − (Al+Si) when the number of cations is based on 22 oxygens, shows that the groundmass phlogopite (ΔT = 0.429–0.666) is enriched in ferric iron relative to the phlogopite macrocrysts (ΔT = 0.01–0.05). The phlogopite aggregates have negative ΔT values, which suggest that they contain no ferric iron in the tetrahedral sites.

Oxide minerals in the kimberlite from the DeBruyn and Martin Mine are represented solely by members of the spinel $MgAl_2O_4$–$FeAl_2O_4$–$MgCr_2O_4$–$FeCr_2O_4$–Fe_3O_4–Fe_2TiO_4 solid solution series (Table 3); magnesium ilmenite, a mineral that is characteristic of most kimberlites, was not observed in kimberlite from DeBruyn and Martin Mine. Spinels occur as both zoned and unzoned crystals. The zoned crystals are mostly idiomorphic (Fig. 1c) and rarely display cores of corroded Mg–Al chromite (Al_2O_3, 5–7 wt.%; TiO_2, 0.75–1.0 wt.%), intermediate zones of titaniferous magnesian chromite (Al_2O_3, 0.7–1.4 wt.%; TiO_2, 3–4.5 wt.%), and rims of titaniferous magnetite (Al_2O_3, 0.04–0.2; TiO_2, 7–7.5 wt.%). Commonly, thin intervening layers of carbonate or serpentine separate magnesian chromite from titaniferous magnetite. In many zoned crystals, Mg–Al chromite is absent, and the core is titaniferous magnesian chromite with a rim of titanomagnetite. Inclusions of groundmass phlogopite are rarely observed in the magnesian chromite, which is sometimes mantled partly by pyrite and partly by serpentine; both sulfide and silicate are mantled by an outer rim of titanomagnetite (Fig. 1d). Some unzoned crystals of euhedral to subhedral titanomagnetite are present and have compositions similar to those of the titanomagnetite rims of the zone crystals.

Perovskite occurs as subhedral to euhedral crystals in the phlogopite-carbonate groundmass. Electron microprobe analyses of perovskite (Table 4) show a remarkable enrichment in REE (12.3–14.53 wt.% RE_2O_3), as well as Nb (2.2–3.0 wt.% Nb_2O_5), relative to other South African kimberlites (Boctor and Boyd, 1980, 1981; Grantham and Allen, 1960).

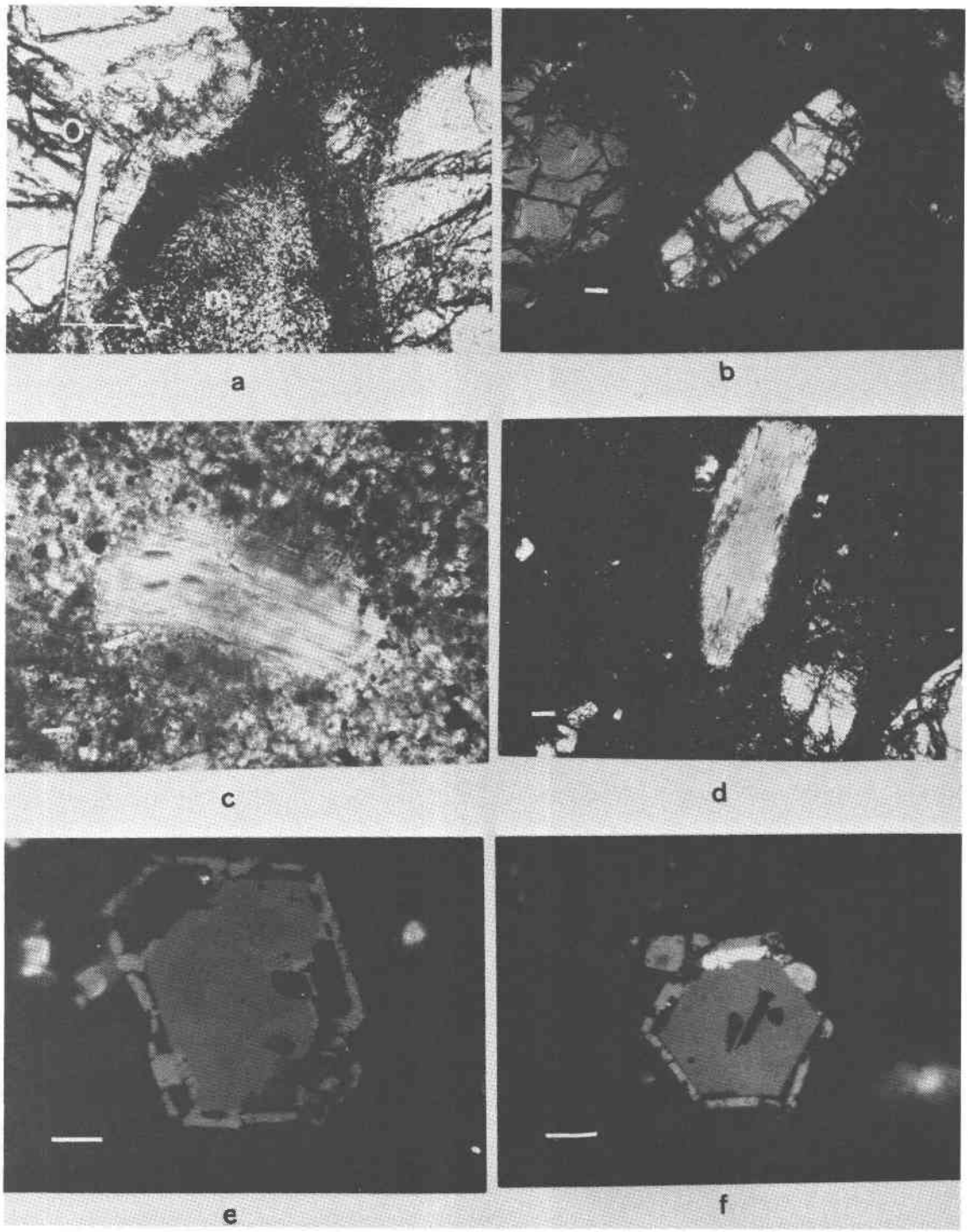

Fig. 1. (a) Portion of a large olivine xenocryst (o) associated with fine-grained mica aggregates (m). Transmitted light; bar = 1 mm. (b) Euhedral crystal of olivine associated with rounded olivine of xenocrystic origin. Transmitted light; bar = 0.1 mm. (c) Sheared phlogopite macrocryst in a calcite-phlogopite groundmass. Transmitted light; bar = 0.05 mm. (d) Zoned phlogopite with clear rims. Transmitted light; bar = 0.01 mm. (e) Corroded Mg–Al chromite rimmed by Mg–Ti chromite and titaniferous magnetite; intervening carbonate (black) exists between Mg–Ti chromite and titaniferous magnetite. Reflected light; bar = 0.02 mm. (f) Euhedral crystal of Mg–Al chromite enclosing inclusions of groundmass phlogopite. The crystal is partly rimmed by pyrite (white) and serpentine (black) and shows an outermost rim of titaniferous magnetite. Bar = 0.02 mm.

Table 1. Representative electron microprobe analyses of olivine and serpentine, wt.%

Oxide	1*	2	3	4	5	6
SiO_2	39.99	40.55	40.61	39.38	39.60	38.92
TiO_2	0.07	<0.01	<0.01	<0.01	0.04	0.25
Al_2O_3	<0.01	0.07	0.05	<0.01	<0.01	0.86
Cr_2O_3	<0.01	<0.01	0.08	0.09	0.30	0.13
MnO	0.24	0.23	0.44	0.13	0.15	0.13
FeO	8.82	8.22	9.88	9.79	9.21	5.60
NiO	0.60	0.32	0.10	0.21	0.21	<0.01
MgO	49.43	49.74	48.48	49.03	49.45	36.02
CaO	0.02	0.05	0.07	0.01	0.06	0.04
	99.11	99.64	99.71	99.28	99.02	82.09
Fo	90.9	91.6	89.7	89.7	90.6	
Fa	9.1	8.4	10.3	10.3	9.4	

**Analyses 1-3; olivine xenocrysts; 4-5, euhedral olivine crystals; 6, serpentine.*

Discussion

The kimberlite from DeBruyn and Martin Mine differs from many South African kimberlites in its lack of magnesium ilmenite, in the compositions and crystallization trends of its spinels, and in the remarkable enrichment of its perovskite in REE. The mineralogy and chemical compositions of the silicate phases in the kimberlite from DeBruyn and Martin Mine, however, are similar to those of other kimberlites.

The olivine xenocrysts are similar in composition to the large, rounded olivines from the Liqhobong kimberlite pipe, which were interpreted as products of disaggregation of ultramafic nodules (Nixon and Boyd, 1973). The occurrence of olivine xenocrysts in association with Cr-rich phlogopite similar to those from lherzolites seems to support their derivation from ultramafic nodules. Olivine phenocrysts, by virtue of their euhedral nature, apparently crystallized from the kimberlite magma. The alteration of olivine to iron-rich serpentine, the lack of magnetite in the serpentinized margins, and the presence of heazlewoodite suggest that the serpentinization process occurred under reducing conditions. Such reducing conditions seem to be characteristic of serpentinization process in kimberlites, as demonstrated by the occurrence of iron-rich serpentines in the Tunraq kimberlite (Mitchell, 1979), in kimberlites from South-West Greenland (Emeleus and Andrews, 1975), and in other micaceous kimberlites (Smith *et al.*, 1978), and also of serpentinization of ultramafic rocks (Ramdohr, 1967).

Two types of phlogopite were identified by Smith *et al.* (1978) in micaceous kimberlites: (1) a very rare iron-rich mica (Mg/(Mg+Fe) = 0.45–0.65; TiO_2, 3–6 wt.%; Al_2O_3, 14–16 wt.%, with no Fe^{3+} in tetrahedral coordination), which they designated as type I; (2) a more abundant Mg-rich mica (Mg/(Mg+Fe) = 0.8–0.93; TiO_2, 0.7–4.0 wt.%; Al_2O_3, 6.8–14.2 wt.%, with Fe^{3+} in tetrahedral sites), which they designated as type II. When the compositions of mica in kimberlite from DeBruyn and Martin Mine are compared with those described by Smith *et al.* (1978), both phlogopite macrocrysts and the groundmass phlogopite are within the compositional ranges for type-II mica. The mica macrocrysts may have crystallized from the kimberlite magma at depth. This suggestion is supported by the experimental investigations of Eggler and Wendlandt (1979) and Wendlandt and Eggler (1980), which indicate that in kimberlitic melts derived by partial melting of garnet lherzolite, phlogopite is stable at pressures above 40 kbar but ceases to be a solidus phase at pressures in excess of 50–55 kbar at 1200° C. The highly deformed nature of the mica megacrysts and the recrystallization effects observed on the borders of some of these crystals also suggest that they crystallized prior to emplacement. Zoned phlogopite macrocrysts that show reverse pleochroism in the cores and normal pleochroism in the rims appear to be of complex origin. Farmer and Boettcher (1981) suggested that the reverse cores were derived from peridotite nodules, whereas the normal rims formed by metasomatic reactions with kimberlitic fluids. The mica aggregates at the contact with round olivine crystals are derived from disaggregated ultramafic nodules. Their compositions are similar to those of micas with secondary textures from lherzolites (Delaney *et al.*, 1980). The groundmass phlogopite has more Ti, total Fe, and Fe^{3+} and is depleted in Al relative to the phlogopite macrocrystas. Because kimberlitic magma tends to become more oxidized and enriched in Ti and Fe with the progress of crystallization and because groundmass phlogopite lacks the deformation features observed in the megacrysts, it is likely that it crystallized from late-stage kimberlitic fluids after emplacement.

The zoning trends of early-formed primary spinels in the so-called "basaltic kimberlite" are consistently from the join $MgCr_2O_4$–$FeCr_2O_4$ to the join $MgAl_2O_4$–$FeAl_2O_4$ with subsequent enrichment in

Table 2. Representative electron microprobe analyses of phlogopite, wt.%*

Oxide	Phlogopite macrocrysts				Phlogopite aggregates		Groundmass phlogopite		
SiO_2	41.56	41.39	39.69**	40.19†	37.30	36.29	39.36	39.61	39.47
TiO_2	0.67	0.68	1.68	3.23	0.71	0.59	1.57	1.57	1.47
Al_2O_3	11.80	11.80	9.45	11.39	14.58	15.18	9.17	9.66	9.78
Cr_2O_3	0.45	0.45	0.54	0.26	2.36	2.70	0.55	0.59	0.62
FeO	3.23	3.03	6.30	6.78	4.75	4.92	6.09	5.90	6.09
NiO	0.17	0.19	0.15	0.18	0.03	0.08	0.13	0.04	0.07
MnO	0.01	0.07	0.05	0.03	0.08	0.21	0.14	0.02	0.03
MgO	25.70	25.66	25.59	22.79	23.23	23.18	25.85	25.39	25.49
CaO	0.03	<0.01	0.10	0.02	<0.01	0.03	0.05	0.04	<0.01
Na_2O	0.13	0.20	0.20	0.09	0.17	<0.01	0.04	0.09	0.05
K_2O	10.27	10.24	8.36	9.13	9.44	9.30	9.17	9.16	9.45
	94.05	93.70	92.13	94.09	92.65	92.48	92.52	92.09	92.32
	Atomic proportions on basis of 22 oxygens								
Si	5.955	5.948	5.875	5.836	5.500	5.379	5.832	5.881	5.629
Ti	0.071	0.071	0.180	0.35	0.078	0.065	0.174	0.174	0.161
Al	1.993	2.000	1.647	1.948	2.531	2.648	1.669	1.690	1.705
Cr	0.054	0.046	0.061	0.030	0.272	0.313	0.061	0.069	0.069
Fe	0.387	0.363	0.778	0.823	0.584	0.608	0.752	0.731	0.752
Ni	0.017	0.024	0.017	0.017	0.00	0.008	0.013	0.004	0.008
Mn	0.00	0.008	0.004	0.00	0.008	0.026	0.013	0.000	0.000
Mg	5.488	5.497	5.646	4.933	5.106	5.118	5.709	5.620	5.629
Ca	0.004	0.00	0.013	0.00	0.00	0.00	0.004	0.00	0.004
Na	0.033	0.055	0.056	0.025	0.047	0.00	0.008	0.013	0.013
K	1.872	1.877	1.577	1.688	1.774	1.757	1.730	1.733	1.783
	15.878	15.888	15.860	15.649	15.900	15.922	15.965	15.928	15.972

**Low totals of the analyses are attributed to the sheared nature of the macrocrysts and the small size of the groundmass phlogopite and phlogopite aggregates.*

***Core.*

†Rim.

total Fe, Fe^{3+}, and Ti. Spinels in micaceous kimberlite from DeBruyn and Martin Mine share with other kimberlitic spinels the overall trend toward enrichment in Fe and Ti (Haggerty, 1975; Mitchell and Clark, 1976), but are generally poor in Al in comparison and show progressive decrease in this element with progressive crystallization. The only other known kimberlitic spinels that show similar depletion in Al_2O_3 are those of micaceous kimberlites from Kirkland (Mitchell, 1978) and from Tun-

Table 3. Representative electron microprobe analyses of spinels, wt.%

Oxide	Mg-Al chromite			Ti-Mg chromite			Titanomagnetite	
	1	2	3	4	5	6	7	8
SiO_2	0.12	0.17	0.18	0.16	0.16	0.24	0.29	0.27
TiO_2	0.76	0.75	1.03	1.91	3.55	4.44	9.30	7.09
Al_2O_3	7.14	7.20	5.37	1.33	1.11	0.66	0.14	0.04
Cr_2O_3	37.43	56.89	55.73	58.50	54.79	50.74	1.16	0.52
Fe_2O_3	7.57	6.41	9.25	9.79	10.65	9.60	55.18	55.22
FeO	14.20	15.72	16.75	16.69	18.55	21.97	26.92	27.22
MnO	0.95	1.03	1.04	1.11	0.94	0.97	1.45	1.29
MgO	11.55	11.09	10.99	10.61	10.46	10.63	5.46	5.32
CaO	0.04	<0.01	<0.01	0.11	0.08	0.12	0.06	0.28
	99.75	99.32	100.90	100.23	100.29	99.33	99.95	99.49

Table 4. Representative electron microprobe analyses of perovskite, wt.%

Oxide	1	2	3	4
SiO_2	0.32	0.27	0.22	0.47
TiO_2	50.21	50.49	50.04	51.71
FeO	1.70	1.90	1.62	1.59
MgO	0.99	0.79	0.37	1.23
CaO	27.91	28.69	27.44	24.54
Na_2O	1.84	1.82	1.54	1.88
La_2O_3	2.41	3.20	2.70	2.14
Ce_2O_3	6.66	6.53	7.90	6.89
Pr_2O_3	0.75	0.30	0.99	0.87
Nd_2O_3	1.53	1.75	1.75	1.96
Sm_2O_3	<0.01	0.03	0.07	<0.01
Eu_2O_3	0.28	0.29	0.23	0.21
Gd_2O_3	0.68	0.74	0.54	0.72
Tb_2O_3	<0.01	<0.01	0.15	<0.01
Dy_2O_3	<0.01	<0.01	<0.01	<0.01
Ho_2O_3	<0.01	<0.01	<0.01	<0.01
Er_2O_3	0.45	0.14	0.20	0.23
Tm_2O_3	<0.01	<0.01	<0.01	<0.01
Yb_2O_3	0.02	<0.01	<0.01	<0.01
Lu_2O_3	0.13	0.09	<0.01	0.21
Nb_2O_5	2.96	2.52	2.18	2.85
	99.25	100.32	98.37	98.27

raq, Canada (Mitchell, 1979). Although limited data are available on spinels from micaceous kimberlites, they seem to have a characteristic compositional trend that involves the crystallization of Al-bearing titaniferous chromite and a progressive decrease in Al and increase in Ti and Fe. In Figure 2 the spinel compositions are plotted in the reduced spinel prism. This type of plot has been used extensively for graphic representation of spinel crystallization trends in kimberlites. Pasteris (1982) suggested that the reduced spinel prism may be misleading because all iron is calculated as Fe^{2+} and that the actual Fe^{2+} should be used in plotting the spinel compositions rather than total Fe calculated as Fe^{2+}. Because $Fe^{2+}/(Fe^{2+}+Mg)$ is used in the plots, the spinels would shift toward more magnesian compositions if Fe^{2+} were used instead of total Fe as Fe^{2+}. The use of the original spinel prism where Fe_3O_4 is an end member is inadequate for representation of Ti-rich kimberlitic spinels because none of the end members is Ti bearing. The use of the spinel prism in the manner adopted in this paper is convenient because it displays the crystallization trends of kimberlitic spinels as shown by their mineral chemistry (compare Fig. 1 and Table 3). It must be understood, however, that the Fe_2TiO_4 end member shows solid solution toward magnetite. The Fe^{2+}/Cr plot favored by Pasteris (1982) does not reflect the crystallization trend displayed by complex spinel solid solutions. It also suffers from the same disadvantage she attributed to the reduced spinel prism because the cations are normalized to the sum of 3 and Fe^{2+} is plotted with against Cr with disregard for the presence of Fe^{3+}; also the substitution of Mg^{2+} for Fe^{2+} and the possible presence of Cr in two different oxidation states are not taken into account. In the reduced spinel prism (Fig. 2), magnesian aluminous chromite and titaniferous magnesian chromite would plot close to the $MgCr_2O_4$–$FeCr_2O_4$ join at the base of the prism, whereas titaniferous magnetite would plot on the triangular face bound by the end members Fe_2TiO_4–$FeCr_2O_4$–$FeAl_2O_4$. The spinel crystallization trend, therefore, is similar to that of lunar spinels (Haggerty, 1972), but differs from that characteristic of mica-poor kimberlites, which generally plot at the base of the spinel prism and at the rectangular face bound by the end members $MgAl_2O_4$–$FeAl_2O_4$–Mg_2TiO_4–Fe_2TiO_4 (Haggerty, 1975). The earliest spinel to crystallize, the magnesian aluminous chromite, represents the primary liquidus spinel that crystallized from the kimberlite magma before emplacement. The crystallization of titaniferous magnesian chromite apparently occurred after the crystallization of groundmass phlogopite, as evidenced by the presence of euhedral inclusions of phlogopite in titaniferous magnesian chromite. The crystallization of groundmass phlogopite prior to titaniferous magnesian chromite depleted the residual kimberlitic fluids in Al, a result which would explain the sharp decrease in Al content of titaniferous magnesian chromite rims relative to the magnesian aluminous chromite cores. The final spinel to crystallize from the residual Fe- and Ti-rich fluids was titanomagnetite, which appears to have crystallized after the beginning of carbonate crystallization in the groundmass and after the onset of serpentinization. This conclusion is suggested by the occurrence of rims of serpentine and carbonate between the inner titaniferous magnesian chromite cores and the outermost titanomagnetite mantles. The euhedral nature of magnesian titaniferous chromite and titanomagnetite and their lack of any indication of resorption or cataclasis suggest that they crystallized after emplacement.

Perovskite in the kimberlite from DeBruyn and

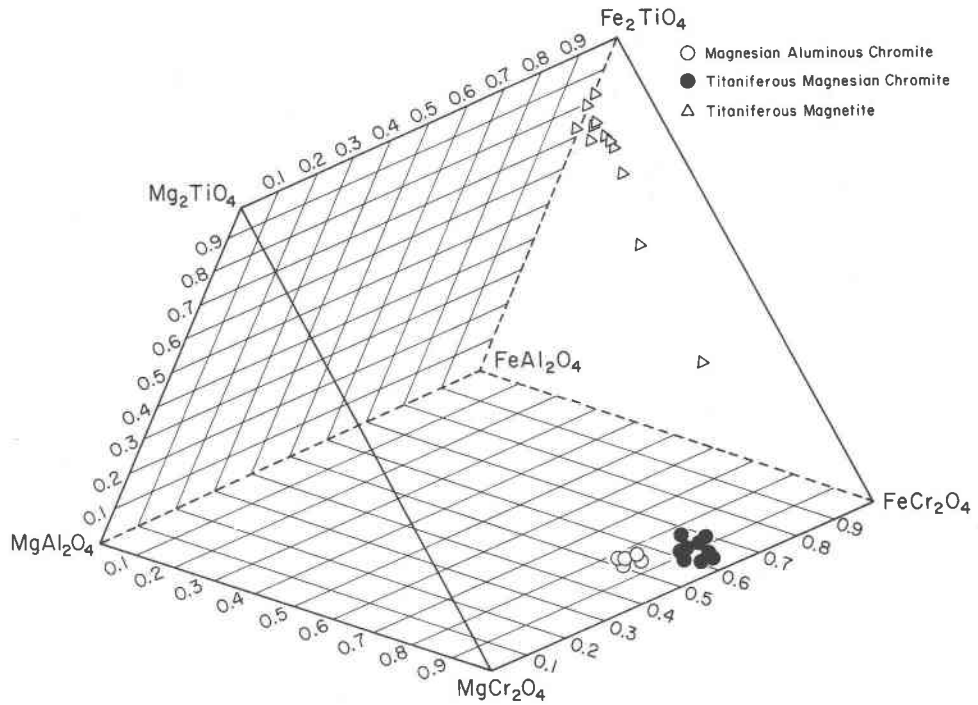

Fig. 2. Compositions of spinels plotted in the reduced spinel prism.

Martin Mine is enriched in REE relative to that of other South African kimberlites (Boctor and Boyd, 1980, 1981; Grantham and Allen, 1960). It also shows the enrichment in LREE characteristic of perovskite in kimberlites and other alkaline rocks. The LREE enrichment in perovskite agrees with the experimental data of Nagasawa *et al.* (1980), who found that the partition coefficient for perovskite-liquid is greater than 2 for LREE and 0.4–0.5 for HREE. Whole-rock analyses of kimberlite from DeBruyn and Martin Mine show that it is highly enriched in REE relative to other South African kimberlites (Fesq *et al.*, 1975). Whole-rock REE patterns for this kimberlite also show a high degree of fractionation, as suggested by the strong LREE enrichment. It can be argued, therefore, that the high total REE content of perovskite from DeBruyn and Martin Mine and its LREE enrichment reflect the high concentrations of REE in the kimberlite magma itself and its highly fractionated nature. The data also suggest that perovskite is the main phase that concentrates REE in kimberlite. An alternative explanation of the LREE enrichment in perovskite is its equilibration with LREE-enriched CO_2 or H_2O vapor, in view of the tendency of these volatiles to be enriched in LREE (Mysen, 1979; Wendlandt and Harrison, 1979).

The high concentrations of REE in kimberlites from the Bellsbank area relative to other South African kimberlites and the large variation in the abundance of these elements in different kimberlites from the Bellsbank group (see Fesq *et al.*, 1975, Table 3) warrant special consideration. Various investigators (Eggler and Wendlandt, 1979; Wyllie, 1979; Mysen and Boettcher, 1975) have suggested that kimberlite magma could be derived from partial melting of garnet lherzolite. Melting relations of an average Lesotho kimberlite (5.2 wt.% CO_2) show that a kimberlite liquid would coexist with an assemblage of Fo + Opx + Cpx + Gar (lherzolite assemblage) at 55 kbar over a temperature range from 1250° C near the solidus to at least 1500° C near the liquidus (Eggler and Wendlandt, 1979). The kimberlite liquid would be enriched in LREE and depleted in HREE. Because of the well known tendency of garnet to concentrate the HREE, the depletion of these elements in the kimberlite liquid can be attributed to equilibration of the liquid with a residuum of garnet peridotite (Eggler and Wendlandt, 1979) or to crystallization and fractionation of garnet from the kimberlitic liquid. Experimental data on the partitioning of REE between garnet and liquid (Mysen, 1978; Harrison, 1981) indicate that garnet fractionation can significantly alter the REE patterns of silicate melts. This effect is even more enhanced in the REE concentration ranges at which

Henry's law does not apply to the garnet phase. As the HREE abundance in the liquid is affected more by deviation from Henry's law than LREE abundance, it is possible to obtain a wide range of LREE-HREE ratios independent of the garnet-to-clinopyroxene ratios in the source (Harrison, 1981). Although garnet fractionation would account for the LREE enrichment observed in the kimberlites from the Bellsbank region, it does not explain the high concentrations of total REE in the Bellsbank kimberlites or the wide variation in total REE among the different kimberlites from the Bellsbank region. A possible explanation for the high REE content of kimberlite magma from Bellsbank is that the garnet lherzolite source was metasomatized. According to Mysen (1979), equilibration of garnet peridotite with water-rich vapor would lead to a wide range of absolute REE content and degrees of LREE enrichment, because the LREE elements tend to concentrate in H_2O vapor. Equilibration of minerals of garnet lherzolite with CO_2 vapor is also likely to lead to LREE enrichment because these elements tend to be remarkably enriched in CO_2 vapor relative to silicate or carbonate liquids (Wendlandt and Harrison, 1979). If the source of the kimberlite magma at Bellsbank was metasomatized garnet lherzolite, partial melting would produce melts enriched in both total REE and LREE. Moreover, the wide variations in the total REE content in different kimberlites from Bellsbank can be attributed to variable degrees of metasomatism of the garnet lherzolite in the source region.

It is interesting to note that the kimberlites from Bellsbank in general and DeBruyn and Martin Mine in particular are also enriched in other incompatible elements such as Nb, Ta, Zr, Hf, and P when compared with "basaltic kimberlites." Moreover, these elements show a wide variation in concentration from one kimberlite to another in the Bellsbank region (Kable *et al.*, 1975). The high concentrations of the incompatible elements in kimberlites from Bellsbank and the tendency of some of these elements to be concentrated by volatiles are consistent with derivation of the kimberlitic magma at Bellsbank from a metasomatized garnet lherzolite source enriched in incompatible elements. This conclusion is supported by the data of Wass and Rogers (1980), which indicate that melting of a metasomatized amphibole- and apatite-bearing garnet lherzolite would lead to concentration of the incompatible elements and the LREE enrichment in the continental alkaline magmas. It is also consistent with the proposal of Boettcher *et al.* (1979) that pervasive metasomatism of upper mantle garnet lherzolite is precursory to or concomitant with partial melting that leads to generation of alkaline basalts and kimberlite magmas.

Acknowledgments

The authors are grateful to Drs. J. J. Gurney, H. S. Yoder, Jr., and an anonymous reviewer for critical comments on the manuscript.

References

Albee, A. L. and Ray, L. (1970) Correction factors for electron microanalysis of silicates, oxides, carbonates, phosphates, and sulfates. Analytical Chemistry, 42, 1408–1414.

Bence, A. E. and Albee, A. L. (1968) Empirical correction factors for the electron microanalysis of silicates and oxides. Journal of Geology, 76, 382–403.

Boctor, N. Z. and Boyd, F. R. (1980) Oxide minerals in the Liqhobong kimberlite, Lesotho. American Mineralogist, 65, 631–638.

Boctor, N. Z. and Boyd, F. R. (1981) Oxide minerals from a layered kimberlite carbonate sill from Benfontein, South Africa. Contributions to Mineralogy and Petrology, 76, 253–259.

Boettcher, A. L., O'Neil, J. R., Windom, K. E., Stewart, D. C. and Wilshire, H. G. (1979) Metasomatism in the upper mantle and the genesis of kimberlite and alkali basalts. In F. R. Boyd and H. O. A. Meyer, Eds., The Mantle Sample, p. 173–182. American Geophysical Union, Washington, D.C.

Bosch, J. L. (1971) The petrology of some kimberlite occurrences in the Barkley West district, Cape Province. Transactions of the Geological Society of South Africa, 74, 75–101.

Colby, J. W. (1971) Magic IV, a computer program for quantitative electron microprobe analysis. Bell Telephone Laboratories, Allentown, Pennsylvania.

Delaney, J. S., Smith, J. V., Carswell, D. A. and Dawson, J. B. (1980) Chemistry of micas from kimberlites and xenoliths—II. Primary and secondary textured micas from peridotite xenoliths. Geochimica et Cosmochimica Acta, 44, 857–872.

Eggler, D. H. and Wendlandt, R. F. (1979) Experimental studies on the relationship between kimberlite magmas and partial melting of peridotite. In F. R. Boyd and H. O. A. Meyer, Eds., The Mantle Sample, p. 330–343. American Geophysical Union, Washington, D.C.

Emeleus, C. H. and Andrews, J. R. (1975) Mineralogy and petrology of kimberlite dyke and sheet intrusions and included peridotite xenoliths from South-West Greenland. Physics and Chemistry of the Earth, 9, 179–197.

Farmer, G. L. and Boettcher, A. L. (1981). Petrologic and crystal-chemical significance of some deep-seated phlogopites. American Mineralogist, 66, 1154–1163.

Fesq, H. W., Kable, E. J. D. and Gurney, J. J. (1975) Aspects of the geochemistry of kimberlite from the Premier Mine and other selected South African occurrences with particular reference to the rare earth elements. Physics and Chemistry of the Earth, 9, 687–734.

Grantham, D. R. and Allen, J. B. (1960) Kimberlites in Sierra Leone. Overseas Geology and Mineral Resources, 8, 5–25.

Haggerty, S. E. (1972) Luna 16—an opaque mineral study and a systematic examination of compositional variations of spinels

from Mare Fecunditatis. Earth and Planetary Science Letters, 13, 328–352.

Haggerty, S. E. (1975) The chemistry and genesis of opaque minerals in kimberlites. Physics and Chemistry of the Earth, 9, 295–307.

Harrison, W. J. (1981) Partition coefficients for REE between garnets and liquids: implications for non-Henry's law behavior for models of basalt origin and evolution. Geochimica et Cosmochimica Acta, 44, 1529–1544.

Kable, E. J. D., Fesq, H. W. and Gurney, J. J. (1975) The significance of inter-element relationships of some minor and trace elements in South African kimberlites. Physics and Chemistry of the Earth, 9, 709–734.

Mitchell, R. H. (1978) Composition of spinels in micaceous kimberlite from the Upper Canada Mine, Kirkland Lake, Ontario. Canadian Mineralogist, 16, 591–595.

Mitchell, R. H. (1979) Mineralogy of the Tunraq kimberlite from the Upper Canada Mine, Kirkland Lake, Ontario. In F. R. Boyd and H. O. A. Meyer, Eds., The Mantle Sample, p. 161–169. American Geophysical Union, Washington, D.C.

Mitchell, R. H. and Clark, D. B. (1976) Oxide and sulfide mineralogy of the Penyuk kimberlite, Somerset Island, N.W.T., Canada. Contributions to Mineralogy and Petrology, 56, 157–172.

Mysen, B. O. (1978) Experimental determination of rare earth element partitioning between hydrous silicate melts, amphibole and garnet peridotite minerals at upper mantle pressures and temperatures. Geochimica et Cosmochimica Acta, 42, 1253–1263.

Mysen, B. O. (1979) Trace element partitioning between garnet peridotite minerals and water-rich vapor; experimental data from 5 to 30 kbar. American Mineralogist, 64, 274–287.

Mysen, B. O. and Boettcher, A. L. (1975) Melting of a hydrous mantle. Journal of Petrology, 16, 520–593.

Nagasawa, H., Schreiber, H. D. and Morris, R. V. (1980) Experimental mineral/liquid partition coefficients of the rare earth elements (REE), Sc, and Sr for perovskite, spinel, melilite. Earth and Planetary Science Letters, 46, 431–437.

Nixon, P. H. and Boyd, F. R. (1973) The Liqhobong intrusion and kimberlitic olivine compositions. In P. H. Nixon, Ed., Lesotho Kimberlite, p. 141–148. Lesotho National Development Corporation, Maseru, Lesotho.

Pasteris, J. D. (1982) Representation of compositions in complex titanian spinels and application to the DeBeers kimberlite. American Mineralogist, 67, 244–250.

Ramdohr, P. (1967) A widespread mineral association, connected with serpentinization. Neues Jahrbuch für Mineralogie, 107, 241–265.

Smith, J. V., Brennesholtz, R. and Dawson, J. B. (1978) Chemistry of micas from kimberlite and xenoliths—I. Micaceous kimberlite. Geochimica et Cosmochimica Acta, 42, 959–971.

Wass, S. Y. and Rogers, N. W. (1980) Mantle metasomatism—precursor to continental alkaline magmatism. Geochimica et Cosmochimica Acta, 44, 1811–1824.

Wendlandt, R. F. and Eggler, D. H. (1980) The origin of potassic magmas: 2. Stability of phlogopite in natural spinel lherzolite and in the system $KAlSiO_4$–MgO–SiO_2–H_2O–CO_2 at high pressures and high temperatures. American Journal of Science, 280, 421–437.

Wendlandt, R. F. and Harrison, W. J. (1979) Rare earth partitioning between immiscible carbonate and silicate liquids and CO_2 vapor: results and implications for the formation of light rare earth enriched rocks. Contributions to Mineralogy and Petrology, 69, 409–419.

Wyllie, P. J. (1979) Kimberlite magmas from the system CO_2–H_2O. In F. R. Boyd and H. O. A. Meyer, Eds., The Mantle Sample, p. 330–343. American Geophysical Union, Washington, D.C.

Manuscript received, December 28, 1981;
accepted for publication, June 8, 1982.